Restoration Strategy for Active Distribution Systems Considering Endogenous Uncertainty in Cold Load Pickup

Yujia Li, *Student Member, IEEE,* Wei Sun, *Member, IEEE,* Wenqian Yin, *Student Member, IEEE,* Shunbo Lei, *Member, IEEE* Yunhe Hou, *Senior Member, IEEE*

Abstract—Cold load pickup (CLPU) phenomenon is identified as the persistent power inrush upon a sudden load pickup after an outage. Under the active distribution system (ADS) paradigm, where distributed energy resources (DERs) are extensively installed, the decreased outage duration can induce a strong interdependence between CLPU pattern and load pickup decisions. In this paper, we propose a novel modelling technique to tractably capture the decision-dependent uncertainty (DDU) inherent in the CLPU process. Subsequently, a two-stage stochastic decision-dependent service restoration (SDDSR) model is constructed, where first stage searches for the optimal switching sequences to decide step-wise network topology, and the second stage optimizes the detailed generation schedule of DERs as well as the energization of switchable loads. Moreover, to tackle the computational burdens introduced by mixed-integer recourse, the progressive hedging algorithm (PHA) is utilized to decompose the original model into scenario-wise subproblems that can be solved in parallel. The numerical test on modified IEEE 123-node test feeders has verified the efficiency of our proposed SDDSR model and provided fresh insights into the monetary and secure values of DDU quantification.

Index Terms—Cold load pickup, decision-dependent uncertainty, distribution system, service restoration, stochastic programming.

NOMENCLATURE

Indices

d, i, l	Indices for loads, buses and distribution lines
g, b, r, e, n	Indices for DG, substation, RES, ESS and DER
t, s	Index for time step and scenario

Sets

$\mathcal{S}$	Set of all scenarios
$\mathcal{T}$	Set of all time steps

$\Omega^D, \Omega^B, \Omega^F$	Set of loads, buses and distribution lines
$\Omega^G, \Omega^{sub}, \Omega^R, \Omega^E$	Set of DGs, substations, RESs and ESSs
$\Omega^{D-SW}, \Omega^{F-SW}$	Set of switchable loads and lines
$\Omega^{G-BS}, \Omega_i^{G-BS}$	Set of blackstart units and those at bus i
$\Omega_i^D, \Omega_i^B, \Omega_i^F \Omega_i^{sub}$	Set of loads, buses, lines and substations at bus i
$\Omega_i^G, \Omega_i^R, \Omega_i^E, \Omega_i^{der}$	Set of DGs, RESs, ESSs and all DERs at bus i

Constant parameters

$\bar{p}_{r,t,s}^{re}$	Forecasted active power output of RES r at time t under scenario s
β_e^c, β_e^d	Charging and discharging efficiency of ESS e
$\check{P}_e^{ess,c}, \hat{P}_e^{ess,c}$	Maximum and minimum active charging power of ESS e
$\check{P}_e^{ess,d}, \hat{P}_e^{ess,d}$	Maximum and minimum active discharging power of ESS e
$\check{P}_g^{dg}, \hat{P}_g^{dg}, \check{Q}_g^{dg}, \hat{Q}_g^{dg}$	Maximum and minimum active/reactive output of DG g
$\check{Q}_r^{re}, \hat{Q}_r^{re}$	Maximum and minimum reactive output of renewable r
$\check{U}_i^{sqr}, \hat{U}_i^{sqr}$	Minimum and maximum squared voltage of bus i
Δt	Length of each time step
$\hat{P}_{b,t}^{sub}$	Maximum active power capacity of substation b from transmission system
$\hat{S}_{ij}$	Rating of distribution line ij
π_s	Probability of scenario s
$P_{d,0}^L, Q_{d,0}^L$	Pre-outage active and reactive power level of load d
r_{ij}, x_{ij}	Resistance and reactance of distribution line ij
RD_g, RU_g	Ramping-up and ramping-down rate of DG g

First-stage decision variables

$\mathcal{Z}_{d,t}$	Binary variable indicating the pickup action of unswitchable load d at time t
$v_{n,t}^{der}$	Binary variable indicating the energizing status of DER n at time t
$v_{g,t}^{dg}, v_{b,t}^{sub}, v_{r,t}^{re}$	Binary variable indicating the operating status of DG g, substation b and RES r at time t
$v_{e,t}^{ess,c}, v_{e,t}^{ess,d}, v_{e,t}^{ess,i}$	Binary variable indicating the charging, discharging and idle status of ESS e at time t
$v_{ij,t}^{line}, v_{i,t}^{bus}$	Binary variable indicating the energizing status of distribution line ij and bus i at time t
$z_{d,t}$	Binary variable indicating the pickup status of unswitchable load d at time t

Second-stage decision variables

$E_{e,t,s}^{ess}$	Residual energy of ESS e at time t under scenario s
$p_{n,t,s}^{der}, q_{n,t,s}^{der}$	Integrated active and reactive output of DER n at time t under scenario s
$p_{g,t,s}^{dg}, q_{g,t,s}^{dg}$	Active and reactive output of DG g at time t under scenario s
$p_{e,t,s}^{ess,c}, p_{e,t,s}^{ess,d}$	Active charging and discharging power of ESS e at time t under scenario s
$p_{ij,t,s}^{line}, q_{ij,t,s}^{line}$	Active and reactive power flow of distribution

	line ij at time t under scenario s
$p_{d,t,s}^{L}, q_{d,t,s}^{L}$	Active and reactive power of load d at time t under scenario s
$p_{r,t,s}^{re,curt}, q_{r,t,s}^{re,curt}$	Curtailment active and reactive power of RES r at time t under scenario s
$p_{r,t,s}^{re}, q_{r,t,s}^{re}$	Active and reactive output of RES r at time t under scenario s
$p_{b,t,s}^{sub}, q_{b,t,s}^{sub}$	Active and reactive power of substation b at time t under scenario s
$U_{i,t,s}^{sqr}$	Squared voltage magnitude of bus i under scenario s
$z_{d,t,s}$	Binary variable indicating the pickup status of switchable load d at time t under scenario s

I. INTRODUCTION

NOWADAYS, ever-increasing extreme events, potentially arising from extreme weather and cyber attacks, have exposed power systems to the underlying threats of large-scale outages [1]. It has been reported that the U.S. needs to spend $18-33 billion every year on dealing with extreme weather events-related outages [2]. Climbing load demands and market deregulation have further accentuated the situation and greatly deteriorated the operation reliability [3]. On the other hand, with the proliferation of active units on the end-users' side, such as distributed energy resources (DERs), energy storage systems (ESSs) and intelligent electronic devices (IEDs), conventional passive distribution systems are gradually evolving into more active ones. In this context, active distribution systems (ADSs) have emerged as powerful tools for realizing self-healing capability [4], relying on which independent service restoration after a major outage becomes realizable even without power support from the external grid [5].

During the service restoration phase of power systems, the occurrence of persistent demand increase arising from cold load pickup (CLPU) has long been a knotty and nonnegligible issue, since the first exploration in 1979 [6]. Physically, the power inrush upon restoration mainly results from the loss of diversity and switching cycle coincidence of process-controlled loads after a sudden power recovery [7]. In some harsh weathers when TCLs take up a high share of total demand, the power inrush can reach up to several times the normal level and last for tens of minutes to hours [6–9]. Therefore, accurate modelling is required to hedge against the potential security issues. Otherwise, adverse effects such as violation of operation limits, equipment damage, and secondary load shedding will occur and delay the restoration process [10]. Currently, the deterministic CLPU model is the most adopted in service restoration, with a pre-fixed set of parameters estimated from historical data [8], [11], [12], or directly computed by simulating the thermal-physical process of thermostatically controlled loads (TCLs) [6], [7]. For instance, a delayed exponent formulation for CLPU is integrated into a multi-time step service model for ADSs in [13]. The associated amplitude and duration of power increase are assumed to be constant throughout the whole restoration period without fluctuation. Similarly, a simplified two-block CLPU model is adopted in [14], with invariant parameters extracted from look-up tables.

Nevertheless, CLPU models based on deterministic parameter-invariant models are no longer applicable for today's ADSs. As ADSs are embracing growing IEDs and DERs, power interruption caused by a major outage can be tackled more swiftly even within several minutes [9]. In this situation, the convergence of TCLs' internal temperature with the ambience is still in progress and their inner thermal-physical properties are changing over time. On the other hand, step-by-step load restoration is prevalent in service restoration to prevent frequency dips and voltage issues. Considering the ongoing process of load undiversification, different energizing orders could lead to distinct CLPU patterns at each load node. While the relationship between CLPU realization and outage duration has long been acknowledged in estimation-related literature [7], [8], limited research in the restoration context has offered an explicit formulation that adequately captures the interdependence between CLPU pattern and sequential load pickup decisions.

Furthermore, another salient obstacle to accurately modelling CLPU is its inherent uncertainty and estimation error. Current CLPU evaluation methods can be mainly categorized into two types, namely physical model-based methods [6], [7], and data-driven statistical methods [8], [11]. For physical model-based methods, the lack of end-user information makes accurate estimation an aporia despite their precision in reflecting the thermal-physical process. For data-driven methods, the random pattern of customer behaviors and regression bias are the main sources of forecast error. On the one hand, because end-users' switching behaviors are random, noise is inevitably introduced into the post-outage load estimation [15]. On the other hand, the limited coverage of sensors and advanced meters in distribution systems adds another dimension of uncertainty to the estimation [16], [17]. According to [8], even after collecting data from 50 instances of historical outages, the percentage error of the CLPU peak exceeds 5%, which will be magnified further if the number of smart meters is reduced and limited outage cases are available. Thus, it is necessary to update existing models to account for the uncertain nature of CLPU.

To tackle the load uncertainty in the restoration problem, stochastic programming (SP) has been extensively used in previous research. In [18], joint probability density functions (PDFs) of renewable outputs during restoration are represented by a Gaussian mixture model. In [19], PDFs are constructed for load and renewable outputs, from which multiple scenarios are generated to discretize PDFs for tractability. Besides the SP, robust optimization (RO) is another commonly adopted modelling method in the same context [9], [20]. With RO, the worst realization of load uncertainty can be identified in a predetermined uncertainty set and then fed into the restoration model to achieve a worst-case immune schedule. However, the majority of the research up to now are designed to quantify the *exogenous uncertainty* of load demand. Specifically, parameters for constructing uncertainty sets or PDFs for exogenous uncertainty are prefixed beforehand and irrelevant to decisions. This fails to work in ADSs, as CLPU uncertainty in the considered context should be classified into *endogenous uncertainty*, which is also named as *decision-dependent un-*
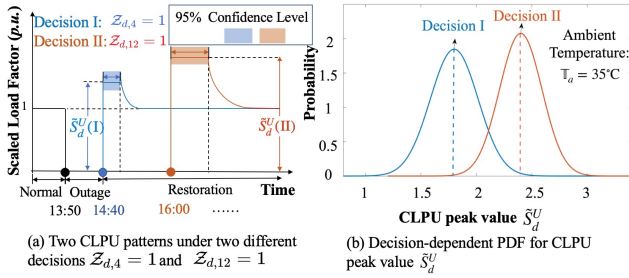
Fig. 1. Motivating example for DDU in CLPU process

certainty (DDU) meaning that uncertainty realization can be affected by decisions. While DDU is rarely examined in the context of restoration, it has been recognized and explored in some power system related areas. For instance, the study in [21] proposes a multistage stochastic planning model that accounts for endogenous uncertainty of customer participation in demand response schemes, and uses Benders decomposition to facilitate computation. In [22], a two-stage resilience enhancement model for distribution systems is constructed, and the DDU of line damage status is linked with first-stage hardening decisions. The progressive hedging algorithm (PHA) is applied to deal with mixed-integer recourse and massive scenarios. Besides, in the field of operation research, several ways to manipulate underlying uncertainties through decision variables have been presented. In [23], distortion toward PDFs is investigated using linear scaling and convex combination of one or more predefined PDFs, which are subsequently incorporated in two-stage stochastic models. The multistage resilient mixed-integer optimization with decision-dependent uncertainty sets is investigated in [24], and nonlinear decision rules are utilized to produce tractable reformulation. The study demonstrates that by appropriately modeling the DDU, the results' conservatism can be mitigated.

To better exemplify the DDU in CLPU, Fig.1 presents a motivating example to show the linkage between load pickup decisions and CLPU evolution patterns, based on the data from [8]. According to Fig. 1(a), after an outage occurs at 13:50, two distinct decisions on load pickup time directly lead to two different CLPU realizations, as the blue and red curves show. Accounting for the inherent stochasticity in estimation, PDFs for the CLPU peak amplitude under these two decisions are presented in Fig.1(b), where an obvious distinction in the expectations and variances can be observed. Under this circumstance, naively adopting an invariant evolution pattern and PDF regardless of load pickup ordering might result in an infeasible restoration schedule and even induce adverse security issues.

Therefore, to precisely capture this DDU, we develop a decision-dependent modelling method for quantifying the interdependence between the CLPU process and load pickup decisions, which is then fed into the subsequent stochastic restoration model.

Based on the above discussions, the major originality and contributions of this paper can be summarized as follows:

1) A novel decision-dependent CLPU (DD-CLPU) model

is proposed considering DDU in the CLPU process. To lessen the computational burden, a technique called mixture distribution is utilized to describe the interdependence of CLPU pattern and load pickup decisions. Through sampling and linearization, tractable reformulation can be obtained without exhausting all possible combinations of load pickup sequences.

2) A two-stage stochastic decision-dependent service restoration (SDDSR) model is constructed with mixed-integer recourse. The first stage decides the optimal switching sequence to determine the step-wise network topology and DERs' startup, based on which detailed operations for DERs are determined in the second stage, upon the DDU of CLPU and exogenous uncertainty of renewable energy sources (RESs) become realized. Switchable loads are considered in the second stage for offering extra flexibility. To relieve computational burdens, the progressive hedging algorithm (PHA) is adopted to solve the large-scale mixed-integer linear programming (MILP) in parallel.

3) To offer fresh insights on the potential value of adopting the decision-dependent method, a useful index, the value of decision-dependent stochastic programming (VDDSS) is computed in the numerical study, under different settings of ambient temperature and outage duration.

The remainder of this paper is organized as follows. Section II presents the DD-CLPU formulation. Section III provides the SDDSR model for ADSs. Section IV illustrates the PHA-based solving method. Numerical results are presented in Section V and Section VI concludes the paper.

II. DECISION-DEPENDENT CLPU MODEL AND TRACTABLE LOAD DEMAND FORMULATION

A. CLPU Issue Triggered by Loss of Load Diversity

Generally, there are three major causes of CLPU problems, including magnetizing inrush during transformation energization, induction motor starting transients, and loss of load diversity [7]. Given that the duration of the first two inrushes is within seconds and can be handled via coordination of protective devices, only the third cause is addressed here.

Load diversity, in the context of this study, refers to the proportion of process-controlled loads with random and independent switching cycles among all loads [25]. During normal operation, the switching actions of process-controlled loads are typically uniformly distributed, allowing them to independently maintain their internal states (such as the temperatures of TCLs) around set-points. However, because their inner states diverged concurrently during the outage, re-energizing the feeder will result in simultaneous switching operations, leading to an abnormal high-level power inrush. To make a clear distinction between these two types of load states, we refer to diversified loads as those that switch independently during normal operation and undiversified loads as those that switch simultaneously after an outage.

B. Decision-Dependent CLPU Model

An accurate model with refined parameters is the preliminary to accurately describe the CLPU properties. It has
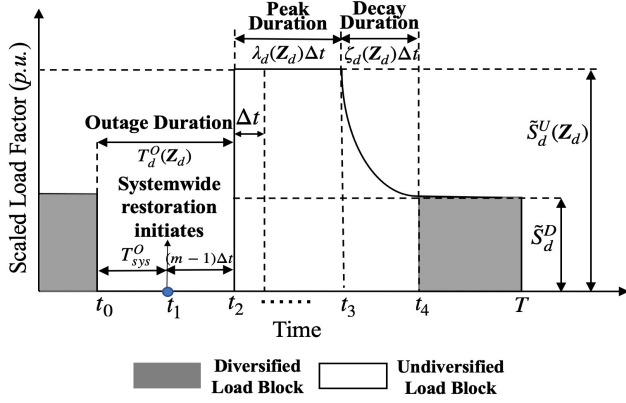
Fig. 2. Decision-dependent Delayed exponential model for feeder-level CLPU

Fig. 3. Regressed scaled CLPU peak value and peak duration against feeder-level outage duration

been recognized that CLPU evolution pattern triggered by loss of load diversity can be approximated by delayed exponent function, where associated parameters are derived from physical method or data-driven method [7]. Fig. 2 depicts the delayed exponent CLPU process with decision-dependent parameters at a certain load feeder. After an outage occurs at t_0, load at node d gradually loses its diversity. When it is restored at t_2, a persistent increase happens and maintains at the peak value for a period of time, as a result of TCLs' simultaneous switching actions. Once the first TCL returns to its preset temperatures at t_3, the feeder-level load begins to decay exponentially until it reaches the pre-outage level at t_4. Physically, this decay is caused by the process of TCLs' diversification, and its duration is highly correlated with the thermal characteristics of buildings and appliances. The associated parameters are defined as below:

$\tilde{S}_d^U(\boldsymbol{Z}_d)$ Stochastic scaled factor of undiversified load d
$\tilde{S}_d^D$ Stochastic scaled factor of diversified load d
$\lambda_d(\boldsymbol{Z}_d)\Delta t$ Peak duration of load d
$\zeta_d(\boldsymbol{Z}_d)\Delta t$ Decay duration of load d
$T_d^O(\boldsymbol{Z}_d)$ Outage duration of load d

where all parameters except $\tilde{S}_d^D$ are parametrized by the decision vector $\boldsymbol{Z}_d = [\mathcal{Z}_{d,1}, .., \mathcal{Z}_{d,|\mathcal{T}|}]$. Note that $\boldsymbol{Z}_d$ is a unit vector with only one non-zero element, as $\mathcal{Z}_{d,t} = z_{d,t} - z_{d,t-1}$ and load is not allowed to be shedded once energized. Here we suppose the demand level after load d completely gains diversity, i.e., $P_{d,0}^L \cdot \tilde{S}_d^D$, only varies around its pre-outage level $P_{d,0}^L$, regardless of its recovery time. This is a mild assumption as outage duration in ADSs is always not long enough for a large discrepancy. Therefore, the mathematical formulation with the defined parameters is stated as below:

$$\tilde{S}_d(t, \boldsymbol{Z}_d) = \tilde{S}_d^U(\boldsymbol{Z}_d) \cdot \left(1 - u(t - t_3(\boldsymbol{Z}_d))\right) \cdot u(t - t_2(\boldsymbol{Z}_d))$$
$$+ \left(\tilde{S}_d^D + (\tilde{S}_d^U(\boldsymbol{Z}_d) - \tilde{S}_d^D) \cdot e^{V(t, \boldsymbol{Z}_d)}\right) \cdot u(t - t_3(\boldsymbol{Z}_d)) \quad (1a)$$

$$V(t, \boldsymbol{Z}_d) = -\alpha_d(\boldsymbol{Z}_d) \cdot (t - t_3(\boldsymbol{Z}_d)) \quad (1b)$$

$$t_2(\boldsymbol{Z}_d) = t_1 + \sum_{m=1}^{|\mathcal{T}|} \boldsymbol{Z}_{d,m} \cdot (m-1) \cdot \Delta t \quad (1c)$$

$$t_3(\boldsymbol{Z}_d) = t_2(\boldsymbol{Z}_d) + \lambda_d(\boldsymbol{Z}_d) \cdot \Delta t \quad (1d)$$

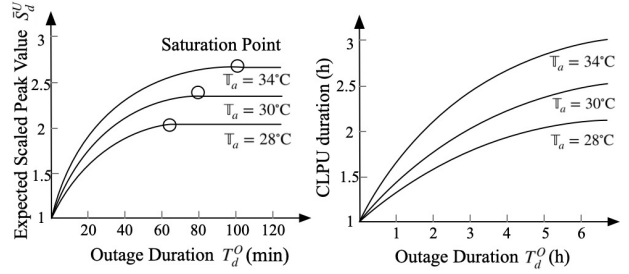where $u(\cdot)$ is the unit step function. The value of $\alpha(\boldsymbol{Z}_d)$

in (1b) duration physically represents the decay rate of the demand level, whose values are strongly correlated with the thermal characteristics of buildings (e.g., thermal capacity and insulation) and TCLs (e.g., rated capacity and temperature thresholds) [6]. The time t_1 when ADS control center initiates restoration is set to be 0. In addition, here we suppose both $\tilde{S}_d^U(\boldsymbol{z}_d)$ and $\tilde{S}_d^D$ follow the Gaussian distribution $\mathcal{N}(\cdot)$:

$$\tilde{S}_d^U(\boldsymbol{Z}_d) \sim \mathcal{N}(\bar{S}_d^U(\boldsymbol{Z}_d,), \sigma_d^U(\boldsymbol{Z}_d)) \quad \forall d \in \Omega^D \quad (2a)$$

$$\tilde{S}_d^D \sim \mathcal{N}(\bar{S}_d^D, \sigma_d^D) \quad \forall d \in \Omega^D \quad (2b)$$

with mean values $\bar{S}_d^U(\boldsymbol{Z}_d)$, $\bar{S}_d^D$ and standard deviations $\sigma_d^U(\boldsymbol{Z}_d)$, σ_d^D. But other forms of PDFs based on ADSs' estimation are also compatible. In this way, the relationship between load pickup decisions and undiversified loading factor is decomposed into two separate parts, which can be conveniently distilled from estimation results. It is worth noting that while σ_d^U and σ_d^D are used to portray CLPU estimation errors, their values can also be adjusted to account for potential biases in load measurements (likely arising from pseudo-measurements [16], [17] due to partially allocated advanced meters or a lack of historical outage cases), uncertainties on the communication side and even to reflect operators' risk aversion. Furthermore, the decision-dependent $\lambda_d(\boldsymbol{Z}_d)$ and $\zeta_d(\boldsymbol{Z}_d)$ are derived from energy not served within the outage time based on estimated $\bar{S}_d^U(\boldsymbol{Z}_d)$, or directly from physical model. Since their stochasticity in time duration is assumed to be comparably smaller than Δt and can be addressed by more prompt control schemes [26], here we supposed them as determinate parameters. Assuming that TCLs account for a significant proportion of overall de-energized loads in the summer, Fig. 3 gives an illustration of regressed relationship between $\bar{S}_d^U(\boldsymbol{Z}_d)$, $\lambda_d(\boldsymbol{Z}_d)$ and $T_d^O(\boldsymbol{Z}_d)$ under different ambient temperature, based on data from [6], [8]. What can be clearly seen in the figure is the nonlinearly increasing trend at the start and the saturation at peak, as the outage proceeds. Since the nonlinearity before saturation points is hard to be tractably incoporated into (1), a step-wise procedure is established to relieve the computational burden in the following subsection.

C. Power Demand Formulation with Sampled DD-CLPU

1) Sampling and Scenario Generation for CLPU parameters: From the above analysis and CLPU modeling, we know that each value of $\boldsymbol{Z}_d$ will result in one specific CLPU curve.

Therefore, we first conduct parameter sampling under each $\boldsymbol{Z}_d$ for discretizing the nonlinear relationship shown as Fig. 3. Then scenario generation is adopted to tackle the intractable PDFs. In summary, the pseudo-code for the detailed procedure is listed in Algorithm 1, and Fig. 4 gives a brief outline of the necessary tasks at each step.

Algorithm 1: Pseudo-code for Parameter Sampling and Scenario Generation

---

1 Obtain the realized parameters: system-wide outage duration T_{sys}^O and ambient temperature $\mathbb{T}_a$;

2 Based on historical CLPU data/appliance information and $\mathbb{T}_a$, estimate associated curves against outage duration, i.e. get explicit expression for $\bar{S}_d^U(T^O)$, $\lambda_d(T^O)$ and $\alpha_d(T^O)$, $\forall d \in \Omega^D$ against outage duration T^O;

3 for $m = 1$ **to** $|\mathcal{T}|$ **do**

4 $\quad T^O(m) = T_{sys}^O + (m-1)\Delta t$

5 end

6 for $\forall d \in \Omega^D$ **do**

7 $\quad$ Fit the estimation error of $\bar{S}_d^U(T^O(m))$ and $\bar{S}_d^D$, here with Gaussian distributions, denoted by $\tilde{e}_d^U(m) \sim \mathcal{N}(0, \sigma_d^U(m))$ and $\tilde{e}_d^D \sim \mathcal{N}(0, \sigma_d^D)$;

8 $\quad$ Calculate $\bar{S}_d^U(m)$, $\lambda_d(m)$ and $\alpha_d(m)$ from estimated curves under $T^O(m)$;

9 $\quad$ Sample $|\mathcal{S}|$ scenarios: $\{e_{d,1}^U(m), .., e_{d,|\mathcal{S}|}^U(m)\}$ from $\mathcal{N}(0, \sigma_d^U(m))$, and $\{e_{d,1}^D, .., e_{d,|\mathcal{S}|}^D\}$ from $\mathcal{N}(0, \sigma_d^D)$;

10 $\quad$ Calculate:

$$\begin{cases} S_{d,s}^U(m) = \bar{S}_d^U(m) + e_{d,s}^U(m) \\ S_{d,s}^D = \bar{S}_d^D + e_{d,s}^D \end{cases} \quad \forall s \in \mathcal{S}$$

11 end

Subsequently, based on the sampled data, each bus node has possible candidate curves with number of $|\mathcal{T}| \times |\mathcal{S}|$, whose formulation can be expressed by discretizing the (1) as below:

$$S_{d,s}(t,m) = S_{d,s}^U(m) \cdot \big(1 - u(t - t_3(m))\big) \cdot u(t - t_2(m)) + \big(S_{d,s}^D + (S_{d,s}^U(m) - S_{d,s}^D) \cdot e^{V(t,m)}\big) \cdot u(t - t_3(m)) \tag{3a}$$

$$V(t,m) = -\alpha_{d,m} \cdot (t - t_3(m)) \tag{3b}$$

$$t_2(m) = (m-1) \cdot \Delta t \tag{3c}$$

$$t_3(m) = t_2(m) + \lambda_{d,m} \cdot \Delta t \tag{3d}$$

$$\forall d \in \Omega^D, m \in \mathcal{T}, s \in \mathcal{S}$$

Mathematically, the curve with index m corresponds to the decision $\boldsymbol{Z}_d$ with element $\mathcal{Z}_{d,m} = 1$. Additionally, it is worth noting that by incorporating historical CLPU data/detailed appliance information, only pre-outage load and post-outage temperature measurements are required for CLPU estimate. As a result, the procedure outlined in this subsection can be carried out offline prior to initiating the restoration. Next, we will show how to establish a tractable load demand formulation using the sampled curves while capturing the decision-dependency.
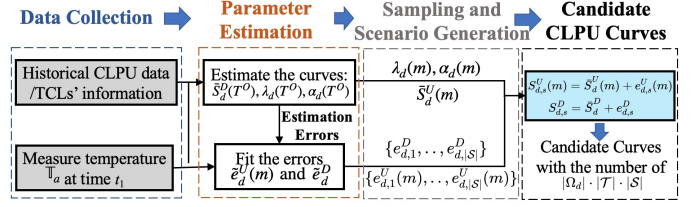

Fig. 4. Procedures for deriving the parameters of candidate CLPU curves

2) Load Demand Formulation with Mixture Distribution: For linearizing the exponent term, each curve presented in (3) is equally sampled with interval Δt:

$$\Delta S_{d,s}(k,m) = S_{d,s}(k\Delta t, m) - S_{d,s}((k-1)\Delta t, m), 1 \leq k \leq |\mathcal{T}|$$

$$\forall d \in \Omega^D, m \in \mathcal{T}, s \in \mathcal{S} \tag{4}$$

The $\Delta S_{d,s}(k,m)$ represents the difference of sampled value at k-th and $(k-1)$-th step of m-th CLPU realization of load d. Then, the scenario-wise load demand is computed as below in an accumulative manner [13]:

$$LF_{d,t,s}(\boldsymbol{Z}_d) = S_{d,s}^U(\boldsymbol{Z}_d)z_{d,t} - \sum_{k=1}^{t} \Delta S_{d,s}^U(\boldsymbol{Z}_d, k)z_{d,t-k+1} \tag{5a}$$

$$\begin{cases} p_{d,t,s}^L(\boldsymbol{Z}_d) = P_{d,0}^L \cdot LF_{d,t,s}(\boldsymbol{Z}_d) \\ q_{d,t,s}^L(\boldsymbol{Z}_d) = Q_{d,0}^L \cdot LF_{d,t,s}(\boldsymbol{Z}_d) \end{cases} \tag{5b}$$

$$\forall d \in \Omega^D, t \in \mathcal{T}, s \in \mathcal{S}$$

where $LF_{d,t,s}(\boldsymbol{Z}_d)$ in (5a) is the time-correlated loading factor of load d at t under scenario s, and decision-dependent coefficients $S_{d,s}^U(\boldsymbol{Z}_d)$ and $\Delta S_{d,s}^U(\boldsymbol{Z}_d, k)$ are defined as below:

$$S_{d,s}^U(\boldsymbol{Z}_d) = \sum_{m=1}^{|\mathcal{T}|} S_{d,s}^U(m)\mathcal{Z}_{d,m} \tag{6a}$$

$$\Delta S_{d,s}^U(\boldsymbol{Z}_d, k) = \sum_{m=1}^{|\mathcal{T}|} \Delta S_{d,s}(k,m)\mathcal{Z}_{d,m} \tag{6b}$$

$$\mathcal{Z}_{d,1} + \mathcal{Z}_{d,2} + .. + \mathcal{Z}_{d,|\mathcal{T}|} = 1 \tag{6c}$$

$$\mathcal{Z}_{d,t} = z_{d,t} - z_{d,t-1} \tag{6d}$$

Without loss of generality, power factors of all load demands are assumed to be fixed during the restoration phase [13], [14], so active and reactive load demand are both directly computed by multiplying the loading factor with their pre-outage levels as (5b) shows. Furthermore, dependency of CLPU realization on load pickup decision is described by (6), through convex combination of sampled $S_{d,s}^U(m)$ and $\Delta S_{d,s}(k,m)$ with respective weight $\mathcal{Z}_{d,m,s}$ ($m = 1, 2, ..|\mathcal{T}|$). In fact, this is a special case for mixture distribution commonly used in decision-dependent stochastic programming [27]. Instead of directly controlling parameters of decision-dependent PDFs, this technique alters PDF pattern by shifting the realized value under each probability level. Specifically, with reference to Fig. 5, through adjusting the controllable weights (here is $\boldsymbol{Z}_d$) of a group of pre-fixed PDFs (here are $|\mathcal{T}|$ discrete PDFs: each consists of $|\mathcal{S}|$ values of $S_{d,s}^U(m)$ and $\Delta S_{d,s}(m)$ with probability π_s), the DDU are tractably captured by outputting different sets of CLPU realizations.
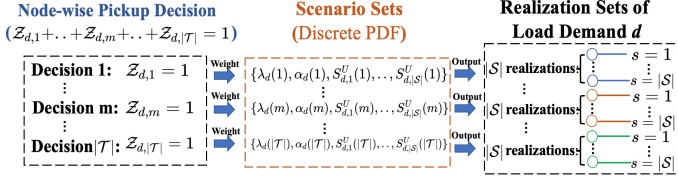
Fig. 5. DDU modelling in load demand formulation with mixture distribution

Subsequently, to tackle the bilinear terms $\mathcal{Z}_{d,m} z_{d,t}$ ($m = 1,..,|\mathcal{T}|$) introduced by the decision-dependent coefficients, auxiliary binary variables $\mathbb{Z}_{d,t,m}(m = 1,..,|\mathcal{T}|)$ are used to linearize each of them[28]:

$$\mathbb{Z}_{d,m,t} \geq \mathcal{Z}_{d,m} + z_{d,t} - 1 \tag{7a}$$

$$\mathbb{Z}_{d,m,t} \leq \mathcal{Z}_{d,m} \tag{7b}$$

$$\mathbb{Z}_{d,m,t} \leq z_{d,t} \tag{7c}$$

and (5a) is reformulated as:

$$LF_{d,t,s} = \sum_{m=1}^{\mathcal{T}} S_{d,m,s}^{U} \mathbb{Z}_{d,m,t} - \sum_{k=1}^{t} \sum_{m=1}^{\mathcal{T}} \Delta S_{d,m,s}(k) \mathbb{Z}_{d,m,t-k+1} \tag{8}$$

Thus, the final formulation for power demand is presented by (4),(5b)-(8). As all terms involving continuous and binary variables have been linearized and the interdependency between the decisions and CLPU uncertainties have been tractably decoupled, it can be directly integrated into the followed MILP-based service restoration model.

III. MATHEMATICAL FORMULATION OF THE TWO-STAGE SDDSR MODEL

A. Assumptions

By combining the above formulated load demand formulation, a two-stage SDDSR model is constructed. Although the main idea behind our proposed DDU-based model is applicable to a wide range of outage scenarios in distribution systems, here we make the following assumptions to narrow down our focus and simplify the exposition:

1) There exists a centralized ADS control center that collects information and optimizes operations. Intelligent electronic devices (IEDs) are distributed throughout the network and conduct measurements. Control commands can be transferred from the control center to ADS devices, such as DERs, lines and load switches.
2) DERs in the studied ADS include dispatchable energy sources, i.e., diesel generators (DGs), energy storage systems (ESSs), and RESs, i.e., wind turbine (WTs) and photovoltaic units (PVs). Uncertainty of RESs' outputs are accounted in the model, by running the Monte Carlo simulation to generate $|\mathcal{S}|$ scenarios for each of them.
3) There only exists one substation or single blackstart unit (BSU) in the considered ADS, and tree topology is maintained through the whole restoration phase. PVs, WTs and ESSs are treated as non-blackstart units (NBSUs) in this paper. Therefore, even though the islanded operation of the ADS as a whole is permitted, the restoration based

on multiple isolated islands is not considered and will be addressed in our future work.
4) Considering that all lines and loads are equipped with remotely-controlled switches is impractical, only a fraction of them are presumed to be switchable. [29]. Furthermore, pickup decisions for switchable loads are made at the second stage to attain extra flexibility.
5) Without loss of generality [5], [13], [14], [20], the studied medium-voltage system is considered to be balanced and represented by its single-phase equivalent circuit.

B. Objective Function

Under the environment of ADS, service restoration has been replenished with new subtasks [19]. Here the objective function includes three terms: the first term is to minimize the total energy not served, with the weighting factor c_d^{ENS} denoting the cost for unit power interruptions. Note that load with higher priority will result in higher c_d^{ENS}. The second term is the operation cost of DGs with unit energy cost c_g^{DG}. The final term is penalty cost for RESs curtailment with unit penalty cost c_r^{RE}, as it is unrealistic to completely accommodate RESs with limited local sources. For not encumbering the load pickup performance, c_d^{ENS} is set to be far higher than the other cost coefficients. The first-stage switching operations are assumed to be cost-free in this study [13], [14].

$$\min \sum_{s \in \mathcal{S}} \pi_s \Big(\sum_{d \in \Omega^D} \sum_{t \in T} c_d^{ENS} S_{d,s}^D P_{d,0}^L (1 - z_{d,t,s}) \Delta t + \sum_{g \in \Omega^G} \sum_{t \in T} c_g^{DG} p_{g,t,s}^{dg} \Delta t + \sum_{r \in \Omega^R} \sum_{t \in \mathcal{T}} c_r^{RE} p_{r,t,s}^{re,curt} \Delta t \Big) \tag{9}$$

C. Stage 1: Determine Optimal Switching Sequence and Restart the BSUs and NBSUs

The outputs of the first stage include start-up decisions for DERs, as well as sequential switching actions for distribution lines. Associated constraints are presented as follows:

$$\sum_{g \in \Omega^{G-BS}} v_{g,1}^{dg} + \sum_{b \in \Omega^{sub}} v_{b,1}^{sub} = 1 \tag{10}$$

$$v_{e,t}^{ess} = v_{e,t}^{ess,c} + v_{e,t}^{ess,d} + v_{e,t}^{ess,i} \leq 1 \quad \forall e \in \Omega^E, t \in \mathcal{T} \tag{11}$$

$$\boldsymbol{v}_{t-1} \leq \boldsymbol{v}_t \quad \forall t \in \mathcal{T} \tag{12}$$

$$z_{d,t-1} \leq z_{d,t} \quad \forall d \in \Omega^D/\Omega^{D-SW}, t \in \mathcal{T} \tag{13}$$

$$v_{n,t}^{der} \leq v_{i,t}^{bus} \quad \forall n \in \Omega_i^{der}, t \in \mathcal{T} \tag{14}$$

$$z_{d,t} = v_{i,t}^{bus} \quad \forall d \in \Omega_i^D/\Omega_i^{D-SW}, t \in \mathcal{T} \tag{15}$$

$$\begin{cases} v_{ij,t}^{line} \leq v_i^{bus} \\ v_{ij,t}^{line} \leq v_j^{bus} \end{cases} \quad \forall ij \in \Omega^{F-RC}, t \in \mathcal{T} \tag{16a}$$

$$\begin{cases} v_{ij,t}^{line} = v_i^{bus} \\ v_{ij,t}^{line} = v_j^{bus} \end{cases} \quad \forall ij \in \Omega^F/\Omega^{F-RC}, t \in \mathcal{T} \tag{16b}$$

$$v_{i,t}^{bus} \leq \sum_{ij \in \Omega_i^F} v_{ij,t}^{line} \quad \forall i \in \Omega^B, t \in \mathcal{T} \tag{17}$$

$$\sum_{ij \in \Omega_i^F} v_{ij,t}^{line} = \sum_{i \in \Omega^B} v_{i,t}^{bus} - 1 \quad \forall t \in \mathcal{T} \tag{18}$$

where constraint (10) enforces one and only one BSU or

substation to be started up at the first time step. Constraint (11) imposes an ESS to operate in one of three modes, namely charging, discharging and idle modes. Given that the major objective of the restoration phase is to restore electricity to end-users as quickly as possible, all DERs and switches except load switches are required to be online once started up or switched, as indicated in (12) and (13). And $\boldsymbol{v}_t$ is the vector that collecting all first-stage energizing variables, i.e., $[v_{1,t}^{der}, .., v_{|\Omega^{der}|,t}^{der}, v_{1,t}^{sub}, .., v_{|\Omega^{sub}|,t}^{sub}, v_{1,t}^{bus}, .., v_{|\Omega^{B}|,t}^{bus}, v_{1,t}^{line}, .., v_{|\Omega^{F}|,t}^{line}]$. Constraints (14)-(17) state the interactions of energizing actions among all components. As there only exists one BSU in the system, constraint (18) together with (10)-(17) sufficiently imposes the tree topology of the network at each step.

D. Stage 2: Finding Optimal Load Pick-up Sequence and Operation Schedule

In the second stage, based on the fixed network and on-state DERs, the schedule for DERs are optimally made under each possible uncertainty realization. Furthermore, switchable loads are adjustable in this stage. Note that as switchable loads also follow the CLPU pattern upon its energization, their pertinent decision variables stated in demand formulation, i.e., (4),(5b)-(8), should be replaced by $z_{d,t,s}, \mathcal{Z}_{d,t,s}$ and $\mathbb{Z}_{d,m,t,s}$ accordingly. Here we do not elaborate the modified formulation for brevity. Thus, except the modified switchable load demand formulation, the second-stage constraints are listed as follows:

$$z_{d,t-1,s} \le z_{d,t,s} \qquad \forall d \in \Omega^{D-SW}, t \in \mathcal{T}, s \in \mathcal{S} \quad (19)$$

$$z_{d,t,s} \le v_{i,t}^{bus} \qquad \forall d \in \Omega_i^{D-SW}, t \in \mathcal{T}, s \in \mathcal{S} \quad (20)$$

$$\sum_{d \in \Omega_i^D} p_{d,t,s}^L + \sum_{ij \in \Omega_i^F} p_{ij,t,s}^{line} - \sum_{ji \in \Omega_i^F} p_{ji,t,s}^{line} = \sum_{n \in \Omega_i^{der}} p_{n,t,s}^{der} + \sum_{b \in \Omega_i^{sub}} p_{b,t,s}^{sub} \quad (21a)$$

$$\sum_{d \in \Omega_i^D} q_{d,t,s}^L + \sum_{ij \in \Omega_i^F} q_{ij,t,s}^{line} - \sum_{ji \in \Omega_i^F} q_{ji,t,s}^{line} = \sum_{n \in \Omega_i^{der}} q_{n,t,s}^{der} + \sum_{b \in \Omega_i^{sub}} q_{b,t,s}^{sub} \quad (21b)$$

$$\forall i \in \Omega^B, t \in \mathcal{T}$$

$$-M \cdot v_{ij,t}^{line} \le p_{ij,t,s}^{line} \le M \cdot v_{ij,t}^{line} \quad (22a)$$

$$-M \cdot v_{ij,t}^{line} \le q_{ij,t,s}^{line} \le M \cdot v_{ij,t}^{line} \quad (22b)$$

$$U_{i,t,s}^{sqr} - U_{j,t,s}^{sqr} \le 2(r_{ij}p_{ij,t,s}^{line} + x_{ij}q_{ij,t,s}^{line}) + M(1-v_{ij,t}^{line}) \quad (23a)$$

$$U_{i,t,s}^{sqr} - U_{j,t,s}^{sqr} \ge 2(r_{ij}p_{ij,t,s}^{line} + x_{ij}q_{ij,t,s}^{line}) + M(v_{ij,t}^{line}-1) \quad (23b)$$

$$\forall ij \in \Omega^F, t \in \mathcal{T}, s \in \mathcal{S}$$

$$v_{g,t}^{dg}\check{P}_g^{dg} \le p_{g,t,s}^{dg} \le v_{g,t}^{dg}\hat{P}_g^{dg}, \forall g \in \Omega^G, t \in \mathcal{T}, s \in \mathcal{S} \quad (24a)$$

$$v_{g,t}^{dg}\check{Q}_g^{dg} \le q_{g,t,s}^{dg} \le v_{g,t}^{dg}\hat{Q}_g^{dg}, \forall g \in \Omega^G, t \in \mathcal{T}, s \in \mathcal{S} \quad (24b)$$

$$RD_g \le p_{g,t,s}^{dg} - p_{g,t-1,s}^{dg} \le RU_g, \forall g \in \Omega^G, t \in \mathcal{T}, s \in \mathcal{S} \quad (25)$$

$$p_{b,t,s}^{sub} \le v_{b,t}^{sub}\hat{P}_{b,t}^{sub} \quad \forall b \in \Omega^{sub}, t \in \mathcal{T}, s \in \mathcal{S} \quad (26a)$$

$$q_{b,t,s}^{sub} \le v_{b,t}^{sub}\hat{Q}_{b,t}^{sub} \quad \forall b \in \Omega^{sub}, t \in \mathcal{T}, s \in \mathcal{S} \quad (26b)$$

$$p_{r,t,s}^{re} = v_{r,t}^{re}\overline{p}_{r,t,s}^{re} \quad \forall r \in \Omega^R, t \in \mathcal{T}, s \in \mathcal{S} \quad (27)$$

$$v_{r,t}^{re}\check{Q}_r^{re} \le q_{r,t,s}^{re} \le v_{r,t}^{re}\hat{Q}_r^{re}, \forall r \in \Omega^R, t \in \mathcal{T}, s \in \mathcal{S} \quad (28)$$

$$0 \le p_{r,t,s}^{re,curt} \le p_{r,t,s}^{re} \quad r \in \Omega^R, t \in \mathcal{T}, s \in \mathcal{S} \quad (29)$$

$$v_{e,t}^{ess,c}\check{P}_e^{ess,c} \le p_{e,t,s}^{ess,c} \le v_{e,t}^{ess,c}\hat{P}_e^{ess,c} \quad (30a)$$

$$v_{e,t}^{ess,d}\check{P}_e^{ess,d} \le p_{e,t,s}^{ess,d} \le v_{e,t}^{ess,d}\hat{P}_e^{ess,d} \quad (30b)$$

$$E_{e,t,s}^{ess} = E_{e,t-1,s}^{ess} + \beta_e^c p_{e,t,s}^{ess,c}\Delta t - \frac{1}{\beta_e^d}p_{e,t,s}^{ess,d}\Delta t \quad (31)$$

$$\check{E}_e^{ESS} \le E_{e,t,s}^{ess} \le \hat{E}_e^{ESS} \quad \forall e \in \Omega^E, t \in \mathcal{T}, s \in \mathcal{S} \quad (32)$$

$$\check{U}_i^{sqr} \le U_{i,t,s}^{sqr} \le \hat{U}_i^{sqr}, \quad \forall i \in \Omega^B, t \in \mathcal{T}, s \in \mathcal{S} \quad (33)$$

$$(p_{ij,t,s}^{line})^2 + (q_{ij,t,s}^{line})^2 \le (\hat{S}_{ij})^2, \forall ij \in \Omega^F, t \in \mathcal{T}, s \in \mathcal{S} \quad (34)$$

$$\sum_{d \in \Omega^D}(p_{d,t,s}^L - p_{d,t-1,s}^L) - \sum_{r \in \Omega^R}(p_{r,t,s}^{re} - p_{r,t-1,s}^{re})$$

$$\le \gamma\big(\sum_{g \in \Omega^G}v_{g,t}^{dg}\hat{P}_g^{dg} + \sum_{e \in \Omega^E}v_{e,t}^{ess,d}\hat{P}_e^{ess,d}\big) \quad \forall t \in \mathcal{T}, s \in \mathcal{S} \quad (35)$$

where constraint (19) and (20) state that the switchable load d cannot be shedded again once picked up, and can only be restored when connecting to an energized node. Constraints (21)-(23) present the linearized DistFlow formulation, where the much smaller nonlinear power loss is neglected [5], [9], [30]. When $v_{ij,t}^{line} = 0$, the constraints (21) ensure that no power flows through line ij, while M is a sufficiently high number to make the constraints trivial when $v_{ij,t}^{line} = 1$. Constraints (23) state the voltage drop between two nodes, and M is used to relax the power flow equation when line ij remains de-energized. Constraints (24) and (25) impose the output limits and inter-temporal ramping rates of DGs, respectively. Constraints (26) state the restorative capacity of substations. For RESs, constraint (27) presents their maximum active power generations under each scenario. Their reactive outputs can be adjusted in certain range to assist in voltage stability, as constraint (28) states. Their curtailment limits are described as (29). Constraints (30) restrict the charging and discharging rates of an ESSs. State of charge (SoC) equation is defined as (31), and the residual energy are limited through (32). Voltage and power flow are restricted within their technical limits, as shown in (33) and (34). To hedge against large frequency dip, a simplified form of frequency response rate (FRR) constraint (35) is used to restrict net load increase at each step, where γ is the FRR factor related to prescribed frequency nadir and set to be 5% in this paper [31].

Therefore, by combining the DDU-based power demand formulation established in last section, the two-stage SDDSR is defined by (4),(5b)-(35). Through linearizing the quadratic constraint (34) via employing two square constraints stated in [20], the final formulation is a large-scale MILP problem with mixed-integer recourse.

IV. Solving method for the DDU-based model

The introduction of stochastic DD-CLPU makes the above-established SDDSR model computationally expensive, especially accounting for the massive second-stage binary variables and scenarios brought by switchable loads. Therefore, the PHA-based decomposition method is adopted here to relieve this burden. PHA is a horizontal decomposition method used for decomposing large-scale stochastic programs to scenario-wise subproblems [32]. Through solving those decomposed subproblems in parallel, the total computation time can be significantly reduced. Although theoretical convergence cannot be strictly guaranteed in MILP case, PHA can still serve as an effective heuristic when discrete variables exist. As Monte Carlo Simulation is applied to generate multiple scenarios for

CLPU and renewable realizations, PHA is naturally applicable in the considered context.

A. Compact form of SDDSR model

To simplify the exposition, the compact form of the two-stage SDDSR model is first derived as below:

$$\min_{\boldsymbol{v}} \boldsymbol{c}^T \boldsymbol{v} + \sum_{s \in \mathcal{S}} \pi_s \varphi(\boldsymbol{v}, s) \tag{36a}$$

$$\text{s.t.} \quad \boldsymbol{A}\boldsymbol{v} \leq \boldsymbol{b}, \quad \boldsymbol{v} \in \{0, 1\}^{n_1} \tag{36b}$$

where vector $\boldsymbol{v}$ represents all binary decision variables in the first stage, and n_1 is the number of those binary variables. $\boldsymbol{c} \in \mathcal{R}^{n_1}$ is the vector for cost coefficients corresponding to $\boldsymbol{v}$. The $\varphi(\boldsymbol{v}, s)$ is the recourse function which can be described as follows:

$$\varphi(\boldsymbol{v}, s) = \min_{\boldsymbol{y}(s), \boldsymbol{z}(s)} \boldsymbol{f}^T \boldsymbol{z}(s) + \boldsymbol{g}^T \boldsymbol{y}(s) \tag{36c}$$

$$\text{s.t.} \quad \boldsymbol{H}(s)\boldsymbol{z}(s) + \boldsymbol{K}\boldsymbol{y}(s) \leq \boldsymbol{d}(s) - \boldsymbol{M}(s)\boldsymbol{x}$$
$$\boldsymbol{z} \in \{0, 1\}^{n_2}, \boldsymbol{y} \in \mathcal{R}^{n_3} \quad \forall s \in \mathcal{S} \tag{36d}$$

where vectors $\boldsymbol{z}$ represents all binary variables in the second stage with the dimension n_2. $\boldsymbol{y}$ is the vector encompassing all continuous variables in the second stage with the dimension of n_3. Vectors $\boldsymbol{f} \in \mathcal{R}^{n_2}$ and $\boldsymbol{g} \in \mathcal{R}^{n_3}$ are the cost coefficient vectors correspond to the $\boldsymbol{z}$ and $\boldsymbol{y}$, respectively. (36d) is the compact form for all second-stage constraints, where $\boldsymbol{H}(s) \in \mathcal{R}^{m_2 \times n_2}, \boldsymbol{K} \in \mathcal{R}^{m_2 \times n_3}, \boldsymbol{d}(s) \in \mathcal{R}^{m_2}$, and $\boldsymbol{M}(s) \in \mathcal{R}^{m_2 \times n_1}$. For distinguishing the original problem with the following decomposed counterpart, the formulation stated as (36) is hereafter referred to as extensive form (EF).

B. Implementation Process of Progressive Hedging Algorithm

For decomposing the EF, $|\mathcal{S}|$ copies of the first-stage variables $\boldsymbol{v}$ are introduced first, then scenario-wise counterpart are subsequently formulated:

$$\min \sum_{s \in \mathcal{S}} \pi_s(\boldsymbol{c}^T \boldsymbol{v}(s) + \boldsymbol{f}^T \boldsymbol{z}(s) + \boldsymbol{g}^T \boldsymbol{y}(s)) \tag{37a}$$

$$\text{s.t.} \quad (\boldsymbol{v}(s), \boldsymbol{z}(s), \boldsymbol{y}(s)) \in \mathcal{W}(s) \tag{37b}$$

$$\boldsymbol{v}(1) = \cdots = \boldsymbol{v}(|\mathcal{S}|) \quad \forall s \in \mathcal{S} \tag{37c}$$

where $\mathcal{W}(s)$ is the feasible set for decision variables under scenario s. Non-anticipative constraint (37c) is introduced to force the convergence of first-stage decisions. Then the pseudo-code for applying PHA on (37) are listed in Algorithm 2, with the following three steps:

Step 1: The iteration of PHA is initialized by setting the iteration count k and multiplier $\boldsymbol{w}^{(k)}(s)$ to 0;

Step 2: $|\mathcal{S}|$ subproblems are solved in parallel to get $\boldsymbol{v}^{(k)}(s)$ under each scenario s. Then the weighted average $\bar{\boldsymbol{v}}^k$ is computed, based on which the $\boldsymbol{w}^{(k)}(s)$ is updated subsequently.

Step 3: Update k. Under each iteration, a well-chosen penalty factor ρ is used to update $\boldsymbol{w}^{(k)}(s)$, which is returned to the objective function of corresponding subproblem in the next iteration. Notice that each subproblem are augmented with a linear term proportional to the multiplier $\boldsymbol{w}^{(k)}(s)$ and

---

Algorithm 2: Pseudo-code of PHA for DDSR model

1 **Step 1.** Let $k = 0$ **and** $\boldsymbol{w}^{(k)}(s) = 0$;
2 **Step 2.** **for** $s = 1$ **to** $|\mathcal{S}|$ **do**
3     $\boldsymbol{v}^{(k)}(s) \leftarrow \arg\min_{\boldsymbol{v}}\big(\boldsymbol{c}^T\boldsymbol{v} + \boldsymbol{f}^T(s)\boldsymbol{z}(s) + \boldsymbol{g}^T\boldsymbol{y}(s) :$
    $(\boldsymbol{v}, \boldsymbol{z}(s), \boldsymbol{y}(s)) \in \mathcal{W}(s)\big);$
4 **end**
5     $\bar{\boldsymbol{v}}^{(k)} \leftarrow \sum_{s \in \mathcal{S}} \pi_s \boldsymbol{v}^{(k)}(s);$
6 **for** $s = 1$ **to** $|\mathcal{S}|$ **do**
7     $\boldsymbol{w}^{(k)}(s) \leftarrow \rho(\boldsymbol{v}^{(k)}(s) - \bar{\boldsymbol{v}}^{(k)});$
8 **end**
9 **Step 3.** **while** $g^{(k)} = \sum_{s \in \mathcal{S}} \pi_s ||\boldsymbol{v}^{(k)} - \bar{\boldsymbol{v}}^{(k)}|| \geq \epsilon$ **do**
10     $k \leftarrow k + 1;$
11   **for** $s = 1$ **to** $|\mathcal{S}|$ **do**
12         $\boldsymbol{v}^{(k)}(s) \leftarrow \arg\min_{\boldsymbol{v}}\big((\boldsymbol{c}^T\boldsymbol{v} + \boldsymbol{w}^{(k+1)}(s)\boldsymbol{v} +$
        $\frac{\rho}{2}||\boldsymbol{v} - \bar{\boldsymbol{v}}^{(k-1)}||^2 + \boldsymbol{f}^T(s)\boldsymbol{z}(s) + \boldsymbol{g}^T\boldsymbol{y}(s) :$
        $(\boldsymbol{v}(s), \boldsymbol{z}(s), \boldsymbol{y}(s)) \in \mathcal{W}(s)\big);$
13   **end**
14     $\bar{\boldsymbol{v}}^{(k)} \leftarrow \sum_{s \in \mathcal{S}} \pi_s \boldsymbol{v}^{(k)}(s);$
15   **for** $s = 1$ **to** $|\mathcal{S}|$ **do**
16         $\boldsymbol{w}^{(k)}(s) \leftarrow \boldsymbol{w}^{(k-1)}(s) + \rho(\boldsymbol{v}^{(k)}(s) - \bar{\boldsymbol{v}}^{(k)});$
17   **end**
18 **end**

---

a squared two norm term penalizing the deviation of $\boldsymbol{v}^{(k)}(s)$ from $\bar{\boldsymbol{v}}^{(k)}$, which can be understood as penalties for not satisfying NAC.

Thus, through solving the decomposed subproblems in a parallel manner, the computation complexity of EF is thus relieved. Its performance in solving the proposed SDDSR model is validated in the numerical test, from the perspectives of accuracy and efficiency.

V. NUMERICAL RESULTS

A. Test System and Data

In this section, the performance of the proposed two-stage SDDSR model is validated via the modified IEEE 123-node test feeders. Based on the network parameters in [33], the studied medium-voltage distribution system is modified to a balanced system, and its single line diagram is depicted in Fig. 6. The unswitchable load nodes and lines are marked in Fig. 6. Here we consider a comparably extreme situation where the ADS has totally lost power support from the substation at node 610 during the whole considered restoration period, due to the substation damage or a major outage originated in the main grid. Under this circumstance, the ADS operator is forced to temporarily form an islanded system by purely utilizing its local sources. Here we assume only the DG at node 27 as a BSU can offer blackstart capability, and node 27 also provides the reference voltage for the whole system. The lower and upper limits of the voltage magnitude are set as 0.95 p.u. and 1.05 p.u., respectively. c_d^{ENS} are randomly generated within the interval between \$2/kWh and \$8/kWh. c_g^{DG} is set as \$0.1/kWh, and c_r^{RE} are equal to \$0.01/kWh. The considered restoration horizon contains 12 steps with a 10-min resolution.
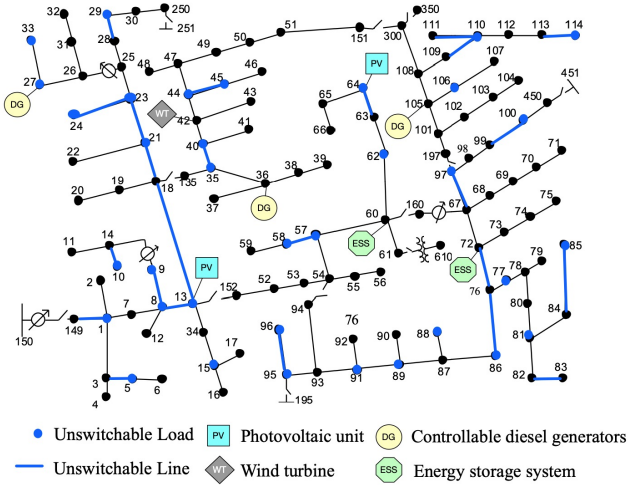
Fig. 6. Modified IEEE 123-node test feeders

Fig. 7. Generated power and percentage restored load under four strategies

TABLE I
DEFINITIONS FOR THE RESTORATION STRATEGIES WITH DIFFERENT
CONSIDERATIONS

Strategy	CLPU Stochasticity	Decision-dependency	Mixed-integer Recourse
I	✓	✓	✓
II	✗	✓	✓
III	✗	✗	✓
IV	✓	✓	✗

As for the CLPU parameter estimation, historical data of CLPU peak value are extracted from [8] and estimated by polynomial regression with saturation at peak. Furthermore, with reference to the simulation results in [9], the peak duration is set as 10, 20, and 30min for the cold load picked up within the time interval $t = 1$ to 4, 5 to 8 and 9 to 12, respectively. As for the decay duration, 10 and 20min are used for cold load that is picked up during the time interval $t = 1$ to 6 and 7 to 12, respectively. Note that the duration can also be calculated by dividing the loss of load energy during the outage with regressed CLPU peak, if sufficient reliable data are available [11]. Assume the blackout occurs in a hot summer day with ambient temperature of 34°C. The control center of ADS initiates restoration 10 min after an unexpected blackout originated from the main grid. Apart from the uncertainty of CLPU, the stochastic nature of WT and PVs should also be considered. For WTs, Weibull distribution [34] and truncated normal distribution [35] are commonly used to quantify the uncertainty of wind speed and power output. Here we adopt the truncated normal distribution to model its output. For PVs, Beta distributions [36] are utilized to portray their stochastic generations. Their expected power outputs are derived from [37] and [38], respectively, with forecast errors set to 10%. 2000 scenarios are generated for uncertain variables by running Monte Carlo simulation, and then reduced to 20 scenarios for tractability [39]. The reformulated MILP problem is performed in Matlab 2021a and solved by Gurobi 9.1 through CVX toolbox, on an Intel Core i5-6500 CPU, 3.2 GHz CPU, 16 GB RAM, and 64-bit operating system PC.
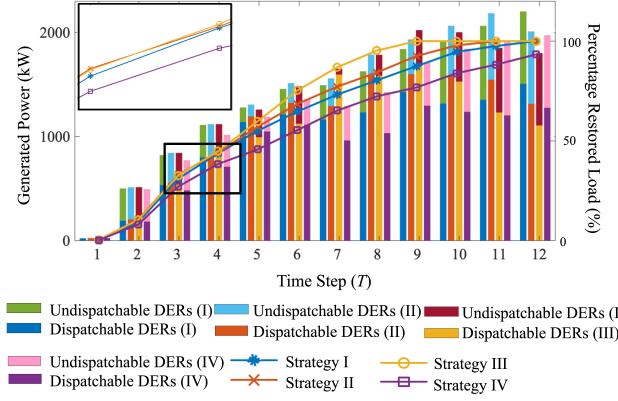
B. Performance of Two-stage SDDSR Strategy

To test the efficiency of our proposed model, four restoration strategies with distinct preliminary knowledge of CLPU are compared. TABLE I presents the different considerations of these four strategies. Strategy I is the restoration plan obtained from our proposed model. Strategy II is extracted by neglecting the stochasticity of the CLPU process, while strategy III totally overlooks the DDU in CLPU. In Strategy IV, the pickup decisions of switchable loads are determined in the first stage, by not allowing for adjustment after uncertainties are realized. To illustrate the expected and actual performance of these four restoration strategies, we show comparisons of their ex-ante and ex-post performances in this subsection.

1) Ex-ante Performance Analysis: First, ex-ante decisions and objective values associated with four stated strategies are evaluated. The term "ex-ante" originates in Latin and means "before the event" [40]. Due to the fact that different scenarios or parameters are given to the CLPU formulation under distinct ex-ante assumptions, the findings reported in this part are their predicted performance (or, alternatively, in-sample performance) with no risk implications or security assurances.

The expected objectives by adopting four strategies are $11324.14, $10284.13, $8107.13 and $13874.28. Fig. 7 depicts the step-wise power generation and accumulated base load restoration in percentage term. As shown by the curves, Strategy III completed the load restoration at $t = 9$, which is much more rapid than strategy I and II who finish re-energization at $t = 11$ and $t = 12$. This shows that the consideration of DDU will delay the restoration process. Strategy II also outperforms Strategy I regarding the expected cost and restoration rate with a comparably smaller gap, as more aggressive switching actions can be made with reduced uncertainty. The pickup progress of strategy IV is behind the other three due to the reduced flexibility. It is worth noting that, while Strategy II and III appear to outperform our proposed strategy I in terms of ex-ant restoration cost and efficiency, their security issues and actual cost cannot be adequately displayed, as will be discussed in the following subsections.

Furthermore, despite the same input of DERs' information and forecast, different generation schedules are observed in the

TABLE II
SECURITY VIOLATIONS OF FOUR STRATEGIES

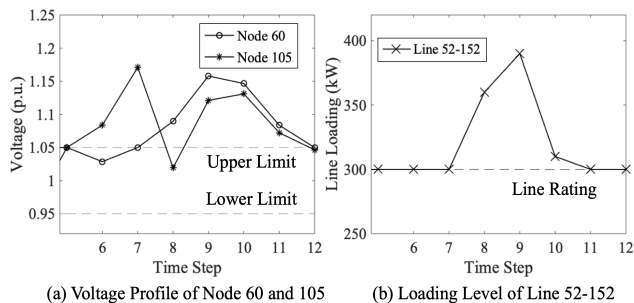| Issues	Strategy	Time step											
		1	2	3	4	5	6	7	8	9	10	11	12
Average bus no. with voltage limits violation	II	0	0	0	0	0	0	0	0	0.9	1.8	1.8	0
	III	0	0	0	0	1.2	1.2	8.5	2.6	3.4	2.2	0.6	0
Average line no. with overloading	II	0	0	0	0	0	0	0	0	1.7	1.1	0.3	0
	III	0	0	0	0	0	3.7	5.9	4.7	2.8	2.2	0	0
Ratio of FRR constraints violation	II	0	0	0	0	0	0	0	0	0	0	0	0
	III	0	0	0	0	0.7%	0.7%	1.9%	1.3%	0	0	0	0

Fig. 8. Voltage Profile of Node 60 and 105 and Loading Level of Line 52-152 (strategy III under test scenario 2)

Fig. 9. VDDSS under different ambient temperature and systemwide outage duration

four strategies. The trivial difference among the generations under strategy I, II and III before $t = 4$ is mainly because the absolute value of load deviation is relatively small due to the light load. Note that for strategy I and II, their overall generation from $t = 6$ to $t = 7$ stay nearly the same even though their restored base load increased, reflecting the diversification of some former-energized load nodes. The decrease in generations after system-wide restoration is completed also shows the decay process of cold load amplitude. Furthermore, while the overall power generation of Strategies I, II, and III is comparable, their load restoration progress is significantly different, due to different ex-ante assumptions about CLPU realizations.

2) Ex-post Performance Analysis and Potential Security Issues: Because the results computed above are all based on distinct ex-ante assumptions, they do not adequately disclose hidden risks in real-world operations. Thus, post-ante (originating from the Latin for "after the event") evaluations are conducted to test their out-of-sample performance. Specifically, by fixing the first-stage solutions of four strategies, i.e., energizing sequences of the network and DERs, we examine their out-of-sample performance using a test set. The test set contains 1000 independent scenarios that are generated by Monte Carlo Simulation to approximate the actual decision-dependent CLPU realizations. For hedging against infeasibility, security and FRR constraints (33)-(35) are relaxed by adding slack variables, which are penalized with high cost in the objective. In this way, the security pitfalls faced by four strategies can be explicitly presented.

TABLE II summarizes the test results in terms of the average number of buses with voltage violations and the average number of lines with overloading. The ratio of FRR constraints that are violated indicates the proportion of scenar-
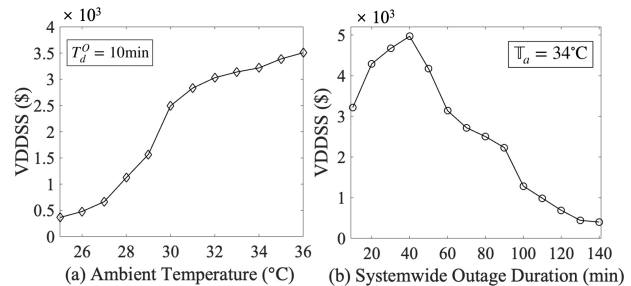
ios with a large frequency dip. It was discovered that under the energizing sequences of strategy I and IV, all test scenarios can be handled without compromising security by using the available flexible measures.

Thus, only the results of Strategy II and III are presented in TABLE II. Violations in voltage and line rating limits are both observed in these two strategies, especially in Strategy III. To show the intensity of the violations, Fig. 8 depicts the voltage profile and line loading level of selected nodes/line under a certain scenario. It is shown that the voltage profile of node 105 rises up to 1.17 p.u at $t = 7$, due to an increased need to deliver more power to balance the underestimated demand than the ex-ante expectation. Moreover, the maximum loading of line 52-152 reached 392.34 kW, about 30% higher than its rating. This is also because PV at node 13 should deliver more power through this line to satisfy the excessive demand which has failed to be accounted under the ex-ante assumption of Strategy III. These results present the potential risks of adopting conventional deterministic CLPU formulation, and demonstrate the importance of properly modelling the DDU of the CLPU process from the perspective of security.

C. The Value of Decisin-Dependent Stochastic Programming under Different Settings

After examining the proposed strategy's security benefits, an effective index, the value of the decision-dependent stochastic programming solution (VDDSS) [41], is introduced to measure the inherent monetary value of the DDU incorporation. To compute this index, first the restoration model with decision-independent PDF for the CLPU process is optimally calculated. Then its first-stage solutions are fed into the SDDSR model and checked by the above-generated test set. Load shedding is permitted here to avoid problem infeasibility, and the corresponding penalty cost is set as 3 times the unit

TABLE III
RESULTS FROM SYSTEMS WITH A DIFFERENT NUMBER OF SWITCHABLE
LOADS

Case	N^{sw}	Obj.($)	T^{res}
1	0	13874.28	14
2	35	11324.14	12
3	70	10159.21	11
4	119	9415.60	11

Fig. 10. Percentage restored load in systems with a different number of switchable loads

TABLE IV
PERFORMANCE RESULTS OF PHA AND EF

	Obj. ($)	Scen.	Ite.	Computation Time
PHA	11324.14	10	4	128s
	11515.73	20	9	723s
	11266.47	50	19	3344s
EF	11324.14	10	-	2478s
	11515.73	20	-	8906s
	-	50	-	-

customer interruption cost. In this way, VDDSS is obtained by subtracting the optimum of the proposed SDDSR model from the optimum of recomputed SDDSR with a fixed first-stage solution derived under decision-independent CLPU.

1) VDDSS under Different Ambient Temperature: The ambient temperature is regarded as a critical factor in determining the post-outage load profile for an ADS with a high penetration of TCLs [7], [9]. Hence, VDDSS is first checked under different ambient temperatures with the same systemwide outage duration of 10 min. Note that although similar results are likely to be observed in a cold winter, here we focus on the hot summer when the ambient temperature is high. Fig. 9(a) shows the result. As the ambient temperature rises, the VDDSS increases accordingly. The slope accelerates at the start, and tends to slow down gradually. The VDDSS is about 30.97% of the objective value under 35°C, but only accounts for 3.21% under 25°C. The growing tendency is mostly due to the fact that TCLs penetrate more extensively at higher ambient temperatures, where they take longer to return to their temperature setpoints.

2) VDDSS under Different Systemwide Outage Duration: This time we vary the systemwide outage duration with a fixed ambient temperature of 34°C. The result is presented in Fig. 9(b). As the outage proceeds, VDDSS increases at first because of the growing CLPU peak. But interestingly, the curve shows a falling trend after peaking at $T^O_{sys} = 40$min. A possible explanation might be that the internal temperature of TCLs has completely converged to the ambience at the tail of restoration phase. In this situation, the interdependency between CLPU pattern and decisions will be naturally decoupled, leading to a reduced value of our DDU-based formulation. It could be further inferred that the VDDSS will gradually converge to zero as the systemwide outage further proceeds.

Therefore, the computation of VDDSS verifies the necessity of utilizing the stochastic decision-dependent restoration model, especially when outage happens under high ambient temperature or a relatively short outage duration. But in the case of systems with light TCL penetration or outages with prolonged duration, it is also acceptable to slightly sacrifice restoration performance for computational tractability.

D. The Impact of Switch Number

This subsection investigates the effect of the switchable loads' number on restoration efficiency. TABLE III summarizes the four cases examined, where N^{sw} in the second column denotes the number of switchable loads and T^{res} in the fourth column is the time steps spent on complete recovery. The switch locations in Case 3 and 4 are picked using the base topology illustrated in Fig. 6.
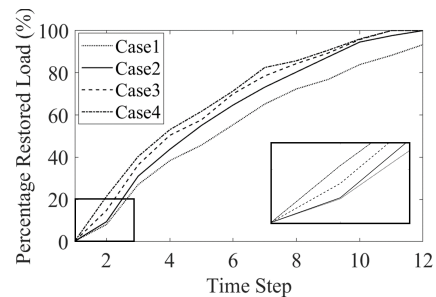
TABLE III shows that as the number of switchable loads increases, the optimal restoration cost reduces. This is a trivial result, as the additional switches enable operators to re-energize spatially dispersed loads to avoid local congestion and voltage violations. But surprisingly, the overall restoration time is not significantly improved, particularly in cases 3 and 4. With reference to Fig. 10, which depicts the percentage restored load at each step, we see that while case 4 initially restores more quickly than case 3, they become almost indistinguishable after $t = 8$. This is because later restored loads that are subjected to larger power inrush cannot be accommodated effectively by simply rearranging the energizing order of switchable loads.

It's also worth mentioning that the switch locations are crucial, as certain switches have greater effects than others. For instance, as illustrated in Fig. 10, the restored load capacity at $t = 2$ is obviously greater in Cases 3 and 4. While the load at node 25 is presumed to be unswitchable in Cases 1 and 2, it is assumed to be switchable in the other two cases. Given that node 25 has a large load capacity, operators can bypass it and subsequently energize the loads located at its downstream nodes if a switch is placed here. Thus, future research may look into the optimal switch allocation problem under a budget constraint.

E. Performance comparison of PHA and EF

Finally, perfomance of PHA is validated by comparing its solving accuracy and efficiency with the EF. As shown in TABLE IV, the objective of PHA-based decomposed model has all converged to the global optimum computed by the EF with acceptable tolerance. Furthermore, computation time has also been greatly reduced by PHA, with a decline of 94.8% and 91.9% under the 10-scenario instance and 20-scenario instance. For 50-scenario instance, no feasible incumbent solution for EF is achieved after 8-hour running, while the

PHA-based decomposed model can still be tackled within acceptable computation time.

VI. CONCLUSION

Accounting for the inherent linkage between the load pickup sequences and the stochastic CLPU process, this paper proposed a two-stage SDDSR model for assisting ADSs in service restoration. Tractable DDU-based load demand formulation is established through parameter sampling and mixture distribution. To tackle the computational complexity induced by DDU modelling and switchable loads, PHA is utilized to relieve the burdens via parallel computing. From numerical studies, we found that the quantification of DDU can greatly shield ADSs from potential security issues, compared with its decision-independent counterparts. Furthermore, the computation of VDDSS illustrates the significance of our proposed DDU-based model, especially under the outage scenario with high TCL penetration and comparably short outage duration. This can also serve as a reliable reference for ADS operators in strategy selection under different outage settings. Finally, PHA is examined as an effective tool for tackling the DDU-based model with mixed-integer recourse, as satisfactory accuracy and reduced running time are both observed. Future studies will examine the impacts of communication-related uncertainty and partial load oberservability, since the coverage rate of smart meters can not be guaranteed in some traditional systems. Additionally, it is desirable to include imbalanced systems and nonlinear properties to achieve more accurate branch flow results. In such cases, relaxation and approximation techniques might be resorted to construct a semidefinite programming (SDP) or second-order conic programming (SOCP) model.

REFERENCES

[1] C. Gillespie, M. Antes, and P. Donnelly, "Climate change and the electricity sector: Guide for climate change resilience planning," 2016.

[2] R. J. Campbell and S. Lowry, "Weather-related power outages and electric system resiliency." Congressional Research Service, Library of Congress Washington, DC, 2012.

[3] S. Tamronglak, S. Horowitz, A. Phadke, and J. Thorp, "Anatomy of power system blackouts: preventive relaying strategies," *IEEE Trans. Power Del.*, vol. 11, no. 2, pp. 708–715, Apr. 1996.

[4] R. Shahin, A. Ali, M. A. Moein, and K. Sajjad, "Load service restoration in active distribution network based on stochastic approach," *IET Gener. Transm. Distrib.*, vol. 12, no. 12, pp. 3028–3036, May 2018.

[5] P. S. Georgilakis, N. C. Koutsoukis, and N. Hatziargyriou, "Service restoration of active distribution systems with increasing penetration of renewable distributed generation," *IET Gener. Transm. Distrib.*, vol. 13, no. 14, pp. 3177–3187, Jun. 2019.

[6] J. E. Mcdonald and A. M. Bruning, "Cold load pickup," *IEEE Trans. Power App. Syst.*, vol. PAS-98, no. 4, pp. 1384–1386, Apr. 1979.

[7] K. P. Schneider, E. Sortomme, S. Venkata, M. T. Miller, and L. Ponder, "Evaluating the magnitude and duration of cold load pick-up on residential distribution using multi-state load models," *IEEE Trans. Power Syst.*, vol. 31, no. 5, pp. 3765–3774, 2015.

[8] F. Bu, K. Dehghanpour, Z. Wang, and Y. Yuan, "A data-driven framework for assessing cold load pick-up demand in service restoration," *IEEE Trans. Power Syst.*, vol. 34, no. 6, pp. 4739–4750, Nov. 2019.

[9] M. Song, R. R. Nejad, and S. Wei, "Robust distribution system load restoration with time-dependent cold load pickup," *IEEE Trans. Power Syst.*, vol. 36, no. 4, pp. 3204–3215, Jul. 2021.

[10] F. Edstrom, J. Rosenlind, K. Alvehag, P. Hilber, and L. Soder, "Influence of ambient temperature on transformer overloading during cold load pickup," *IEEE Trans. Power Del.*, vol. 28, no. 1, pp. 153–161, Dec. 2012.

[11] S. Dzeletovic, F. Bouffard, H. Michalska, and G. Joós, "Regression-based wintertime energy consumption prediction for cold load pick-up management," in *Proc. IEEE Power and Energy Soc. General Meeting*, Aug. 2020, pp. 1–5.

[12] C. Hachmann, G. Lammert, L. Hamann, and M. Braun, "Cold load pickup model parameters based on measurements in distribution systems," *IET Gener. Transm. Distrib.*, vol. 13, no. 23, pp. 5387–5395, Nov. 2019.

[13] B. Chen, C. Chen, J. Wang, and K. L. Butler-Purry, "Multi-time step service restoration for advanced distribution systems and microgrids," *IEEE Trans. Smart Grid*, vol. 9, no. 6, pp. 6793–6805, Nov. 2018.

[14] A. Arif, S. Ma, Z. Wang, J. Wang, S. M. Ryan, and C. Chen, "Optimizing service restoration in distribution systems with uncertain repair time and demand," *IEEE Trans. Power Syst.*, vol. 33, no. 6, pp. 6828–6838, Nov. 2018.

[15] S. Lefebvre and C. Desbiens, "Residential load modeling for predicting distribution transformer load behavior, feeder load and cold load pickup," *Int. J. Electr. Power Energy Syst.*, vol. 24, no. 4, pp. 285–293, May 2002.

[16] J. Zhao, C. Huang, L. Mili, Y. Zhang, and L. Min, "Robust medium-voltage distribution system state estimation using multi-source data," in *2020 IEEE Power & Energy Society Innovative Smart Grid Technologies Conference (ISGT)*. IEEE, May 2020, pp. 1–5.

[17] B. P. Hayes, J. K. Gruber, and M. Prodanovic, "A closed-loop state estimation tool for mv network monitoring and operation," *IEEE Trans. Smart Grid*, vol. 6, no. 4, pp. 2116–2125, Dec. 2014.

[18] Z. Wang, C. Shen, Y. Xu, F. Liu, X. Wu, and C.-C. Liu, "Risk-limiting load restoration for resilience enhancement with intermittent energy resources," *IEEE Trans. Smart Grid*, vol. 10, no. 3, pp. 2507–2522, May 2019.

[19] F. Shen, Q. Wu, J. Zhao, W. Wei, N. D. Hatziargyriou, and F. Liu, "Distributed risk-limiting load restoration in unbalanced distribution systems with networked microgrids," *IEEE Trans. Smart Grid*, vol. 11, no. 6, pp. 4574–4586, May 2020.

[20] X. Chen, W. Wu, and B. Zhang, "Robust restoration method for active distribution networks," *IEEE Trans. Power Syst.*, vol. 31, no. 5, pp. 4005–4015, 2016.

[21] S. Giannelos, I. Konstantelos, and G. Strbac, "Option value of demand-side response schemes under decision-dependent uncertainty," *IEEE Trans. Power Syst.*, vol. 33, no. 5, pp. 5103–5113, 2018.

[22] S. Ma, L. Su, Z. Wang, F. Qiu, and G. Guo, "Resilience enhancement of distribution grids against extreme weather events," *IEEE Trans. Power Syst.*, vol. 33, no. 5, pp. 4842–4853, 2018.

[23] L. Hellemo, P. I. Barton, and A. Tomasgard, "Decision-dependent probabilities in stochastic programs with recourse," *Comput. Manag. Sci.*, vol. 15, no. 3, pp. 369–395, Aug. 2018.

[24] W. Feng, Y. Feng, and Q. Zhang, "Multistage robust mixed-integer optimization under endogenous uncertainty," *Eur. J. Oper. Res.*, vol. 294, no. 2, pp. 460–475, Oct. 2021.

[25] F. Friend, "Cold load pickup issues," in *2009 62nd Annual Conference for Protective Relay Engineers*. IEEE, May 2009, pp. 176–187.

[26] V. Kumar, I. Gupta, and H. O. Gupta, "An overview of cold load pickup issues in distribution systems," *Electr. Power Compon. Syst.*, vol. 34, no. 6, pp. 639–651, Feb. 2006.

[27] L. Hellemo, P. I. Barton, A. Tomasgard, and R. Schultz, "Decision-dependent probabilities in stochastic programs with recourse," *Computational Management Science*, vol. 15, no. 3-4, pp. 369–395, 2018.

[28] F. Glover and E. Woolsey, "Further reduction of zero-one polynomial programming problems to zero-one linear programming problems," *Oper. Res.*, vol. 21, no. 1, pp. 156–161, Feb. 1973.

[29] S. Lei, Y. Hou, F. Qiu, and J. Yan, "Identification of critical switches for integrating renewable distributed generation by dynamic network reconfiguration," *IEEE Trans. Sustain. Energy*, vol. 9, no. 1, pp. 420–432, Jan. 2018.

[30] S. Lei, C. Chen, Y. Song, and Y. Hou, "Radiality constraints for resilient reconfiguration of distribution systems: Formulation and application to microgrid formation," *IEEE Trans. Smart Grid*, vol. 11, no. 5, pp. 3944–3956, 2020.

[31] B. Zhao, X. Dong, and J. Bornemann, "Service restoration for a renewable-powered microgrid in unscheduled island mode," *IEEE Trans. Smart Grid*, vol. 6, no. 3, pp. 1128–1136, May 2015.

[32] J. P. Watson and D. L. Woodruff, "Progressive hedging innovations for a class of stochastic mixed-integer resource allocation problems," *Computational Management Science*, vol. 8, no. 4, pp. 355–370, 2011.

[33] W. H. Kersting, "Radial distribution test feeders," *IEEE Trans. Power Syst.*, vol. 6, no. 3, pp. 975–985, Aug. 1991.

[34] C. Ozay and M. S. Celiktas, "Statistical analysis of wind speed using two-parameter weibull distribution in alaçatı region," *Energy Conversion*

and Management, vol. 121, pp. 49–54, Aug. 2016.

[35] Y. V. Makarov, P. V. Etingov, J. Ma, Z. Huang, and K. Subbarao, "Incorporating uncertainty of wind power generation forecast into power system operation, dispatch, and unit commitment procedures," *IEEE Trans. Sustain. Energy*, vol. 2, no. 4, pp. 433–442, Jun. 2011.

[36] S. Velamuri and S. Sreejith, "Economic dispatch and cost analysis on a power system network interconnected with solar farm," *Int. J. Renew. Energy Res.*, vol. 5, no. 4, pp. 1098–1105, 2015.

[37] "NREL. Solar power data for integration studies," Available: https://www.nrel.gov/grid/solar-power-data.html.

[38] "NREL. Wind Integration National Dataset Toolkit," Available: https://www.nrel.gov/grid/wind-toolkit.html.

[39] N. M. Razali and A. Hashim, "Backward reduction application for minimizing wind power scenarios in stochastic programming," in *2010 4th International Power Engineering and Optimization Conference (PEOCO)*. IEEE, 2010, pp. 430–434.

[40] S. Mitra, "A white paper on scenario generation for stochastic programming," *Optirisk systems: white paper series, ref. No. OPT004*, 2006.

[41] Y. Zhan, Q. P. Zheng, J. Wang, and P. Pinson, "Generation expansion planning with large amounts of wind power via decision-dependent stochastic programming," *IEEE Trans. Power Syst.*, vol. 32, no. 4, pp. 3015–3026, Jul. 2016.

Shunbo Lei (M'17) received the B.E. degree in electrical engineering and automation from Huazhong University of Science and Technology, Wuhan, China, in 2013, and the Ph.D. degree in electrical and electronic engineering from The University of Hong Kong, Hong Kong SAR, in 2017. He was a visiting scholar at Argonne National Laboratory, Lemont, IL USA, from 2015 to 2017, a postdoctoral researcher with The University of Hong Kong from 2017 to 2019, and a research fellow with the University of Michigan, Ann Arbor, MI USA, from 2019 to 2021. He is currently an assistant professor with the School of Science and Engineering, The Chinese University of Hong Kong, Shenzhen, China, and also visiting with the University of Michigan. His research interests include power systems, resilience, grid-interactive efficient buildings, optimization and learning.
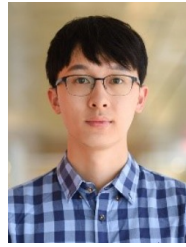
Yujia Li (S'19) received her B.E. degree in electrical engineering and automation from Huazhong University of Science and Technology, Wuhan, China, in 2018. She is currently pursuing the Ph.D. degree with the Department of Electrical and Electronic Engineering, The University of Hong Kong, Hong Kong, China. Her current research interests include resilient operation and planning of distribution systems, and renewable integration.

Wei Sun is currently an Associate Professor in the Department of Electrical and Computer Engineering at the University of Central Florida. He is also the Director of Siemens Digital Grid Lab. He received his Ph.D. degree from Iowa State University in 2011. His research interests include power system restoration, self-healing smart grid, and cyber-physical system security and resilience.

Yunhe Hou (M'08-SM'15) received the B.E. and Ph.D. degrees in electrical engineering from Huazhong University of Science and Technology, Wuhan, China, in 1999 and 2005, respectively. He was a Post-Doctoral Research Fellow at Tsinghua University, Beijing, China, from 2005 to 2007, and a Post-Doctoral Researcher at Iowa State University, Ames, IA, USA, and the University College Dublin, Dublin, Ireland, from 2008 to 2009. He was also a Visiting Scientist at the Laboratory for Information and Decision Systems, Massachusetts Institute of Technology, Cambridge, MA, USA, in 2010. He has been a Guest Professor with Huazhong University of Science and Technology, China from 2017 and an Academic Adviser of China Electric Power Research Institute from 2019. He joined the faculty of the University of Hong Kong, Hong Kong, in 2009, where he is currently an Associate Professor with the Department of Electrical and Electronic Engineering. Dr. Hou is an Editor of the IEEE Transactions on Smart Grid and an Associate Editor of the Journal of Modern Power Systems and Clean Energy.

Wenqian Yin (S'18) received the B.E. in electrical engineering from Jiangsu University, Zhenjiang, China, in 2015 and the M.S. degree in electrical engineering from Hohai University, Nanjing, China, in 2018. She is currently working toward the Ph.D. degree in electrical engineering at The University of Hong Kong, Hong Kong, China. Her research interests include power system operation and planning, and renewable energy.